Nanoscale

ROYAL SOCIETY OF CHEMISTRY

COMMUNICATION

View Article Online
View Journal | View Issue

Check for updates

Cite this: *Nanoscale*, 2020, **12**, 5332

Received 28th December 2019,
Accepted 10th February 2020

DOI: 10.1039/c9nr10921h

rsc.li/nanoscale

Employing bicontinuous-to-micellar transitions in nanostructure morphology for on-demand photo-oxidation responsive cytosolic delivery and off–on cytotoxicity†

Sharan Bobbala,‡[a] Sean D. Allen,‡[b] Sijia Yi,[c] Michael Vincent,[a] Molly Frey,[b] Nicholas B. Karabin[a] and Evan A. Scott *[a,b,c,d]

Bicontinuous nanospheres (BCNs) are underutilized self-assembled nanostructures capable of simultaneous delivery of both hydrophilic and hydrophobic payloads. Here, we demonstrate that BCNs assembled from poly(ethylene glycol)-*block*-poly(propylene sulfide) (PEG-*b*-PPS), an oxidation-sensitive copolymer, are stably retained within cell lysosomes following endocytosis, resisting degradation and payload release for days until externally triggered. The oxygen scavenging properties and enhanced stability of the bicontinuous PEG-*b*-PPS nanoarchitecture significantly protected cells from typically cytotoxic application of pro-apoptotic photo-oxidizer pheophorbide A and chemotherapeutic camptothecin. The photo-oxidation triggered transition from a bicontinuous to micellar morphology overcame this stability, allowing on-demand cytosolic delivery of camptothecin for enhanced control over off–on cytotoxicity. These results indicate that inducible transitions in the nanostructure morphology can influence intracellular stability and toxicity of self-assembled nanotherapeutics.

Introduction

A key rationale for specifying the nanostructure of drug delivery vehicles is to beneficially alter the pharmacodynamics and biodistribution of loaded cargo molecules.[1] By altering the size and morphology, the employed nanostructure may increase on-target delivery and reduce off-target uptake of their bioactive payloads.[2] Despite these well-documented benefits, nanostructure-mediated delivery still results in non-specific cellular uptake, particularly by cells of the mononuclear phagocyte system in organs such as the liver and spleen.[3] This presents a particular challenge when potent cytotoxic cargoes are delivered. Stimuli-responsive nanostructures may decrease such non-specific cytotoxicity by providing spatiotemporal control over cargo release.[4]

One difficulty in using stimuli-responsive nanostructures is that they are often fabricated *via* the self-assembly of block copolymers, resulting in sensitive and easily ruptured vehicles. In particular, nanocarriers with aqueous lumens, which are required for facile encapsulation and transport of both hydrophilic and hydrophobic payloads simultaneously, are quickly disrupted under the harsh conditions of intracellular compartments.[5] For example, despite their known enhanced stability relative to liposomes during *in vivo* transport, polymersomes are equally unlikely to survive intact within the lysosome for more than a few hours regardless of their chemistry. Here, we utilize a highly stable self-assembled polymeric nanocarrier morphology known as a bicontinuous nanosphere (BCN), which is characterized by a cubic lattice of aqueous channels that traverse its hydrophobic interior volume.[6] BCNs are the polymeric equivalent of lipid cubosomes, and their organized, lyotropic and interconnected internal architecture make them exceptionally robust and stable assemblies, relative to polymersomes, when loading high concentrations of molecular cargo.[7]

BCNs self-assembled from poly(ethylene glycol)-*block*-poly(propylene sulphide) (PEG-*b*-PPS) are capable of loading both hydrophilic and hydrophobic compounds simultaneously, making them a versatile drug delivery vehicle.[7,8] PEG-*b*-PPS nanocarriers of varying morphology successfully deliver cargo *in vitro* and *in vivo* with a demonstrated lack of toxicity in both murine and non-human primate models.[7,9–13] The hydro-

[a]*Department of Biomedical Engineering, Northwestern University, Evanston, Illinois 60208, USA. E-mail: evan.scott@northwestern.edu*
[b]*Interdepartmental Biological Sciences Program, Northwestern University, Evanston, Illinois 60208, USA*
[c]*Chemistry of Life Processes Institute, Northwestern University, Evanston, Illinois 60208, USA*
[d]*Simpson Querrey Institute, Northwestern University, Chicago, Illinois 60611, USA*

†Electronic supplementary information (ESI) available: Experimental details, Fig. S1: additional confocal images, S2: low magnificent TEM micrograph, S3: change in turbidity of BCNs upon irradiation, S4: singlet oxygen generation at high power, S5: photo-oxidation induced release of hydrophilic cargo, S6: ROS generation upon irradiation of cells, S7: low magnification TEM micrograph of irradiated supernatant, S8: micelle diameter distribution from TEM micrographs, S9: confocal images of PhA FITC-BSA BCNs co-localized with lysotracker. See DOI: 10.1039/C9NR10921H

‡These authors contributed equally to this work.

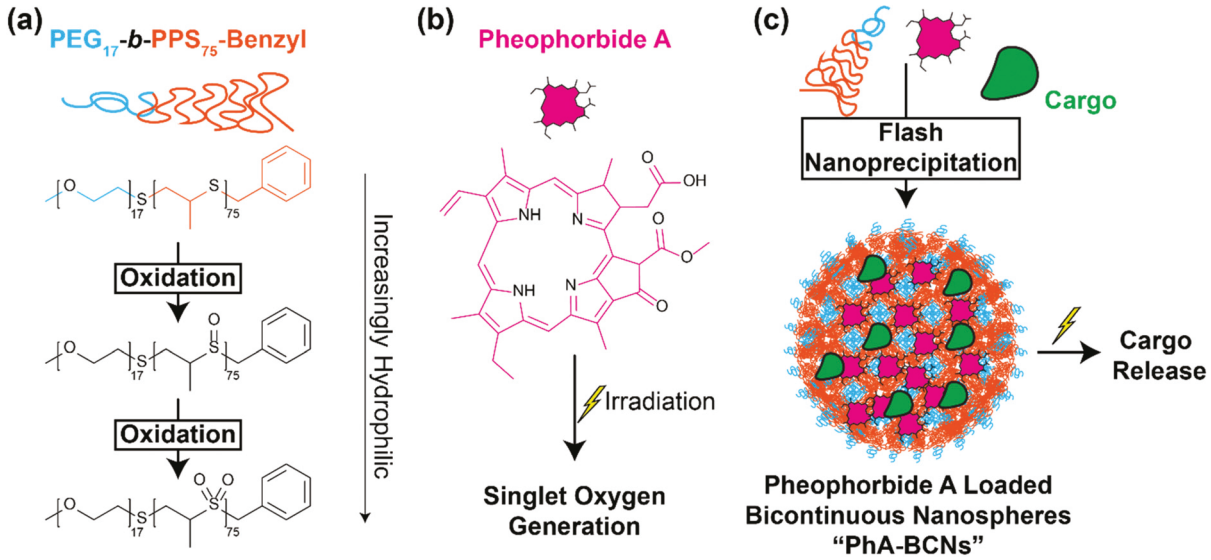

Scheme 1 Formation of PhA-loaded BCNs (PhA-BCNs) from oxidation-sensitive PEG-*b*-PPS polymer. (a) PEG-*b*-PPS polymer structure. Sulfide oxidation into sulfoxide and sulfone groups increases hydrophilicity. (b) Pheophorbide A structure. (c) BCN self-assembly and cargo loading were performed using flash nanoprecipitation (FNP).

phobic PPS block of the polymer can be oxidized into sulfoxide and sulfone derivatives under physiological conditions, leading to an increase in the hydrophilicity of the block and resulting disassembly of PEG-*b*-PPS nanostructures, including BCNs (Scheme 1a).[14] This oxidation-based alteration in the hydrophilic mass fraction of the diblock copolymer drives morphological changes in the aggregate nanostructure, and it has previously been demonstrated that this morphological change can result in the release of cargo from PEG-*b*-PPS nanostructures.[12] We have previously demonstrated that PEG-*b*-PPS filomicelles and polymersomes transition into micelles upon photo-oxidation triggered degradation,[12,14] but how this process impacts intracellular delivery of BCN has not been previously explored.

We hypothesized that PEG-*b*-PPS BCN nanocarriers would stably retain cargo even upon internalization by cells due to their enhanced nanoarchitecture-dependent stability.[7] Furthermore, we reasoned that their large hydrophobic PPS volume may serve as a dense sponge for enhanced scavenging of reactive oxygen species (ROS),[15] providing BCNs with sensitivity to photo-oxidizers for triggered release but without associated ROS-induced cytotoxicity. To test this, we loaded BCNs with the cytotoxic photosensitizer pheophorbide A (PhA) and assessed its ability to safely induce intracellular degradation of BCNs. Co-loading of BCNs with PhA and cytotoxic chemotherapeutics demonstrated an off–on on-demand photosensitive cytotoxicity (Scheme 1b), verifying that the BCN nanoarchitecture could retain cytotoxic payloads intracellularly with extended cell viability. Such capability may allow usage of more sensitive and a wider range of photosensitizers during photo-triggered intracellular delivery as well as decrease off-target side effects associated with photodynamic nanotherapy.

Results and discussion

To investigate the ability of BCNs to stably retain cargo within cell endosomal compartments, we encapsulated fluorescein-tagged bovine serum albumin (FITC-BSA) within BCNs using flash nanoprecipitation (FNP). FNP is currently the only scalable technique capable of forming uniform spherical BCNs and loading them with hydrophilic and hydrophobic compounds (Scheme 1c).[8,11,16] Free FITC-BSA was rapidly endocytosed by phagocytic RAW 264.7 cells, forming small punctae that colocalized with a lysosomal stain (Fig. 1a). These FITC-BSA punctae decreased in intensity over the course of 48 h, likely due to pH-dependent degradation of the fluorophore and the BSA, which is known to occur rapidly.[17,18] In contrast, BCN-encapsulated FITC-BSA retained fluorescence intensity within endosomes (Fig. S1†) well beyond 48 h and was still visible within cells 168 h (7 days) after internalization (Fig. 1b). Overall, the intracellular retention at the 168 h timepoint for BCN-loaded FITC-BSA was comparable to free FITC-BSA after 48 h. The persistence of fluorescent punctae confirmed using lysotracker red and lack of FITC-BSA cytosolic signal strongly suggests that BCNs aid in the stable retention of cargo within the lysosomes of cells. Indeed, quantification of fluorescent signal from cells demonstrates that while free FITC-BSA signal was higher at the early 4 h time point compared to FITC-BSA BCNs, it was significantly lower than the FITC-BSA BCN signal at 48 h (Fig. 1c). This precipitous decline in free FITC-BSA intracellular signal is not seen with FITC-BSA encapsulated within BCNs between 4 h and 48 h (Fig. 1c). To further confirm this phenomenon, BCNs were loaded with a BODIPY-BSA and intracellular degradation was quantified over a 24 h period. BODIPY-BSA utilizes a quenched fluorophore, which increases in fluorescence as the BSA is degraded until

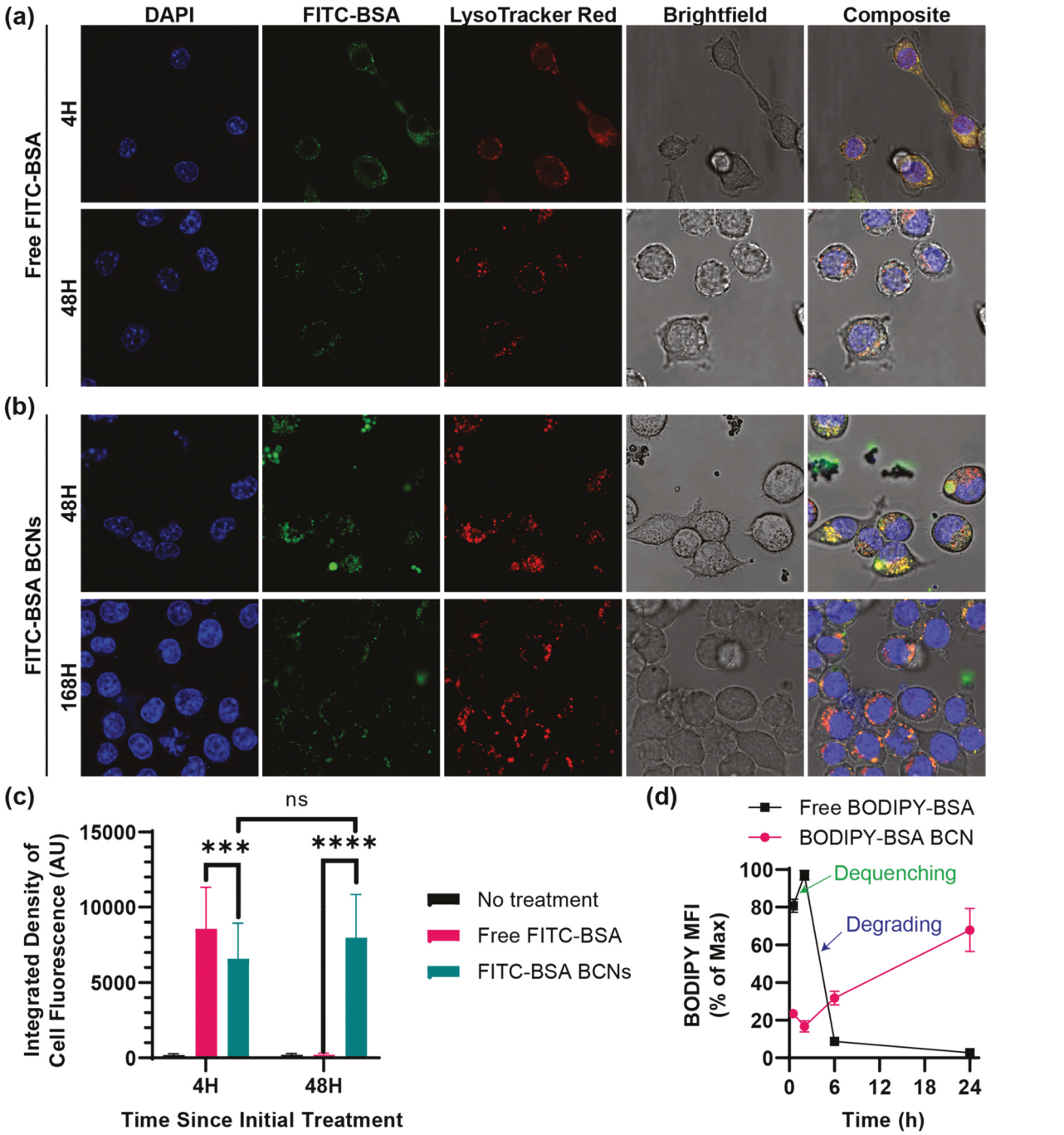

Fig. 1 Subcellular localization and retention of free or encapsulated FITC-BSA. (a) Representative confocal micrographs of RAW 264.7 cells immediately after a 4 h incubation with FITC-BSA or 48 h after a 4 h incubation with FITC-BSA. (b) Representative confocal micrographs of RAW 264.7 cells after 48 or 168 h after a 4 h incubation with BCNs loaded with FITC-BSA. All cells were stained with NucBlue for nuclei and LysoTracker Red for lysosomes, magnification 40× objective lens. (c) Integrated density of fluorescent signal for randomly selected cells that underwent no treatment or treatment with either free FITC-BSA or FITC-BSA BCNs. Data was obtained for 30 cells per condition and 3 separate experiments using ImageJ Software. Cells were analyzed immediately after a 4 h incubation with treatment or 44 h after a 4 h incubation with treatment (48 h total). Statistical analysis was performed using 2-way ANOVA, ***$p < 0.001$ and ****$p < 0.0001$. (d) Flow cytometric analysis of BODIPY fluorescence in RAW 264.7 cells at various timepoints after a 30-minute BODIPY-BSA BCN incubation ($n = 4$; error bars = s.d.).

the BODIPY itself degrades. Free BODIPY-BSA treated cells demonstrated a rapid increase in fluorescence that peaked within 2 h, indicating the nearly immediate degradation of the BSA and resulting dequenching of the BODIPY fluorophores (Fig. 1d). This was followed by a gradual decline in fluorescence as the fluorophore is processed and cleared by the cells. In contrast, BODIPY-BSA encapsulated in BCNs demonstrated a very gradual increase in fluorescence and never

peaked over the 24 h period of the study, indicating retarded degradation of the BSA.

We next sought to probe the stimuli-responsiveness of BCNs by co-encapsulating a photo-oxidizer. We chose pheophorbide A (PhA), known to produce singlet oxygen and ROS at such high levels that it is typically employed to induce cell death for cancer applications.[19,20] PhA is a relatively hydrophobic molecule ($\log P$ = 6.93), which correlates well with high encapsulation efficiency in PEG-*b*-PPS nanostructure systems.[8,11,13,21] However, encapsulation of hydrophobic cargoes can at times disrupt the aggregate morphology of nanostructures, so we assessed the PhA-loaded BCN (PhA-BCN) formulations for their morphological characteristics.[7] Negative-stained transmission electron micrographs (TEM) showed that PhA-BCNs retained their characteristic morphology (Fig. 2a and S2†). DLS analysis of the formulations found a diameter of 245.8 ± 11.6 nm and a PDI of 0.15 ± 0.02, which was in good agreement with previous studies on the characteristics of PEG-*b*-PPS BCNs.[7,8] Formulations were also analysed by small-angle X-ray scattering for Bragg peaks at the $\sqrt{2}$, $\sqrt{4}$, and $\sqrt{6}$ ratios, indicating that their primitive cubic type (*Im*3*m*) internal organization was preserved (Fig. 2b).[6] As expected for its hydrophobicity, PhA was encapsulated at a high efficiency of 80.7 ± 2.2%. Hydrophilic cargo was simultaneously encapsulated with PhA into BCNs for release studies (Fig. 2c). Agreeing with previously published results, loading of hydrophilic payloads into BCNs is size dependent, with FITC-BSA outperforming calcein encapsulation, 34 ± 4% *vs.* 6.7 ± 1.9%, respectively.[8]

Photo-oxidation of PEG-*b*-PPS nanostructures had previously been explored using the photo-oxidative fluorophore ethyl eosin.[8,14] Other nanostructures, such as polymersomes and filomicelles, appeared to readily release cargo upon photo-oxidation with ethyl eosin, but BCNs contain considerably more PPS in their interior volume and may therefore require a stronger photo-oxidizer. We therefore compared the ability of ethyl eosin and PhA to induce photo-oxidation-triggered degradation of BCNs. After irradiation of a solution of BCNs loaded with photo-oxidizer, the samples were centrifuged to pellet the intact BCNs for sampling of the supernatant. PhA was released into the supernatant in significantly greater amounts than the comparably ineffective ethyl eosin (Fig. 2d and S3†), verifying the superior capacity of PhA to generate the oxidation required for degradation of the dense BCN nanoarchitecture. These results also demonstrated the high stability of BCN and their ability to resist degradation under conditions that would normally rupture polymersomes.[14] Upon irradiation, free PhA significantly decreased the absorbance of DPBF, a probe for singlet oxygen generation (Fig. 2e and S4†). Blank BCNs, *i.e.* BCNs which were not loaded with PhA, showed no effect on DPBF absorbance. Encapsulation of PhA in BCNs did not inhibit the generation of singlet oxygen, with PhA-BCNs demonstrating significantly more singlet oxygen generation than blank BCNs (p < 0.0001). This generation of singlet oxygen was able to trigger the release of cargo from BCNs loaded with both PhA and a hydrophilic molecule – either calcein or FITC-BSA. After irradiation, BCNs were centrifuged

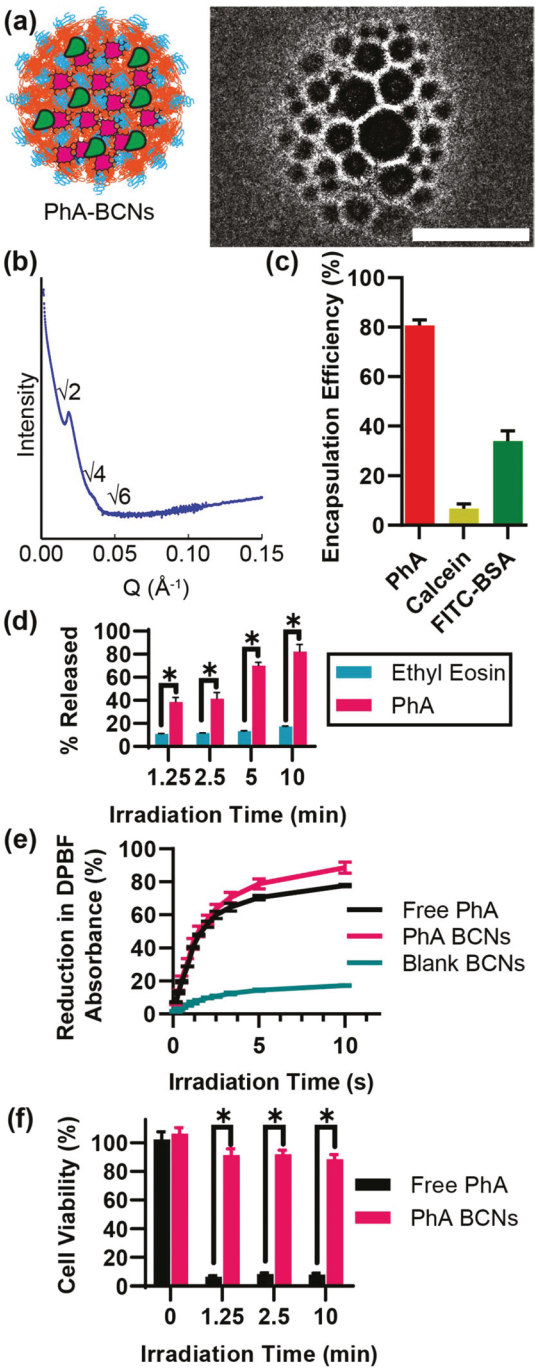

Fig. 2 Physical characterization of PhA-BCNs. (a) TEM micrograph of PhA-BCN. Scale bar = 100 nm. (b) SAXS curve of PhA-BCN, with labelled Bragg peaks. (c) Encapsulation efficiency of PhA and hydrophilic cargoes calcein and FITC-BSA (n = 3, error bars = s.d.). (d) Percentage of fluorescence signal in the supernatant after irradiation and centrifugation of BCNs loaded with PhA or ethyl eosin, n = 4, error bars = s.d. (e) Generation of singlet oxygen assayed by percent decrease in DPBF absorbance for free solubilized PhA, blank BCNs, and PhA-BCNs (n = 4, error bars = s.d.). (f) MTT assay of cell viability with or without irradiation for cells treated with free PhA or PhA-BCNs, 12 h after irradiation. For all subfigures *p < 0.0001.

into a pellet and the supernatant containing released cargo was removed. The pellet was resuspended and assayed for the presence of cargo. Both hydrophilic cargoes were rapidly released from BCNs upon irradiation, most likely due to the destabilization of the BCN morphology allowing for release from the internal aqueous channels (Fig. S5a†). This release of cargo, determined by measuring the decrease in fluorescence of the sample, was corrected for any photobleaching effects (Fig. S5b†).

The most common application of PhA is as a photodynamic therapy agent for generating cytotoxic ROS in anti-cancer applications.[19] Indeed, free PhA with very brief irradiation was able to promote significant cell death in RAW 264.7 cells (Fig. 2f). In contrast, PhA-BCNs demonstrated little, though statistically significant ($p < 0.001$), decrease in cell viability after the same duration of irradiation compared to non-irradiated cells, despite forming similar levels of singlet oxygen (Fig. 2e). This difference in ROS generation (Fig. S6†) is likely due to the

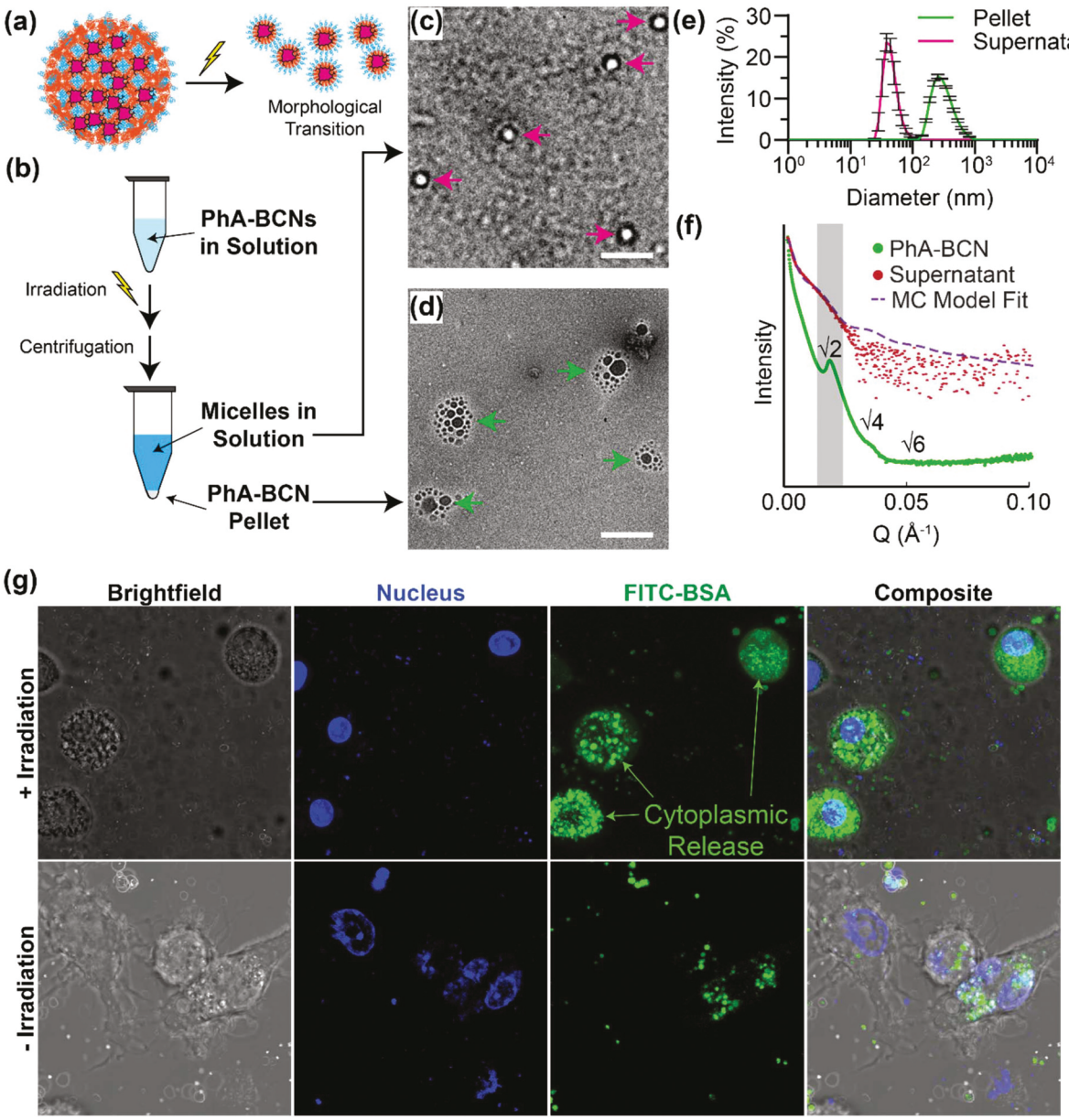

Fig. 3 Morphological transition of BCNs into micelles by photo-oxidation. (a) Diagram of PhA-BCNs degrading into micelles after irradiation. (b) Schematic of BCN isolation from micelles by centrifugation at 10 000 rcf. (c) TEM micrograph of micelle nanostructures isolated from the supernatant of centrifuged samples after irradiation. (d) TEM micrograph of BCNs isolated from the pellet of centrifuged samples after irradiation. Scale bar of TEM micrographs = 200 nm. (e) DLS size distributions of samples shown in (c) and (d) (n = 3, error bars = s.d.). (f) SAXS curve of the supernatant shown in (c), shown with the SAXS curve of non-irradiated PhA-BCNs (same curve as shown in Fig. 2b). Supernatant SAXS data was fitted with a micelle model fit using SASView. SAXS data was arbitrarily offset between BCN and supernatant data. (g) Confocal images of PhA-BCNs loaded with FITC-BSA, internalized by RAW 264.7 cells, with or without irradiation, magnification 63× objective lens.

rapid consumption of singlet oxygen species by PPS,[15] which effectively scavenged ROS in the immediate area where they are being formed.

In PEG-*b*-PPS polymersome and filomicelle systems, photooxidation triggers morphological changes, ultimately resulting in the formation of micelle structures.[12,14] We hypothesized that a similar morphological transition would occur for photooxidized BCNs (Fig. 3a). To investigate, we sought to enrich for the morphological transition products by exploiting the propensity of the highly dense BCNs to pellet upon centrifugation (Fig. 3b). Examination of the supernatant and pellet using TEM revealed that the supernatant contained micellar structures while the pellet contained BCNs (Fig. 3c, d and S7†). Dynamic light scattering (DLS) size distributions showed a reduction in the diameter of nanostructures after irradiation, representing a shift from larger BCNs to smaller micelles (Fig. 3e), which was also seen after quantification of nanostructure diameters *via* TEM (Fig. S8†). This change in aggregate structure was corroborated by SAXS data, which revealed changes in scattering upon irradiation, particularly the loss of the high intensity crystalline $\sqrt{2}$ Bragg peak in the supernatant (Fig. 3f). The supernatant SAXS scattering profile was best fit (χ^2 = 0.0005) by a micelle model with core radius of 16.8 nm. Since micellar structures contain a hydrophobic core and are unable to load hydrophilic molecules, this transition from BCN to micelle presents an explanation for the rapid release of hydrophilic cargo after irradiation of PhA-BCNs.

Although often difficult to achieve without cytotoxicity, cytosolic delivery of endosomal payloads is particularly useful for a variety of therapeutic applications, including vaccination.[9,22] A number of mechanisms have been employed to traverse endosomal membranes, the majority of which induce lysosomal rupture and release of previously sequestered toxic enzymes and ions.[23] In contrast, PEG-*b*-PPS nanostructures have been found to deliver payloads to the cytosol *via* temporarily increasing endosomal membrane permeability and without toxicity.[9,14] For polymersomes, this process involves the oxidation and resulting increased hydrophilicity of the PPS block (Scheme 1a), which triggers a thermodynamically driven conversion from stable vesicles to unstable micelles capable of fusing with and permeabilizing neighbouring membranes for milliseconds.[14] We hypothesized that the morphological transition of BCNs and contemporaneous release of hydrophilic cargo could similarly destabilize endosomal compartments to also allow release of hydrophilic cargo into the cytosol. As a qualitative assessment of this hypothesis, PhA FITC-BSA BCNs, *i.e.* BCNs co-encapsulating both PhA and FITC-BSA, were incubated with RAW 264.7 cells. Cells were repeatedly washed to remove BCNs that were not internalized and subsequently irradiated prior to confocal imaging. Both irradiated cells and non-irradiated controls contained green fluorescent punctae representing BCNs and cargo localized within the endolysosomal pathway (Fig. 3g and S9†). Non-irradiated cells only featured fluorescence within these punctae, reminiscent of

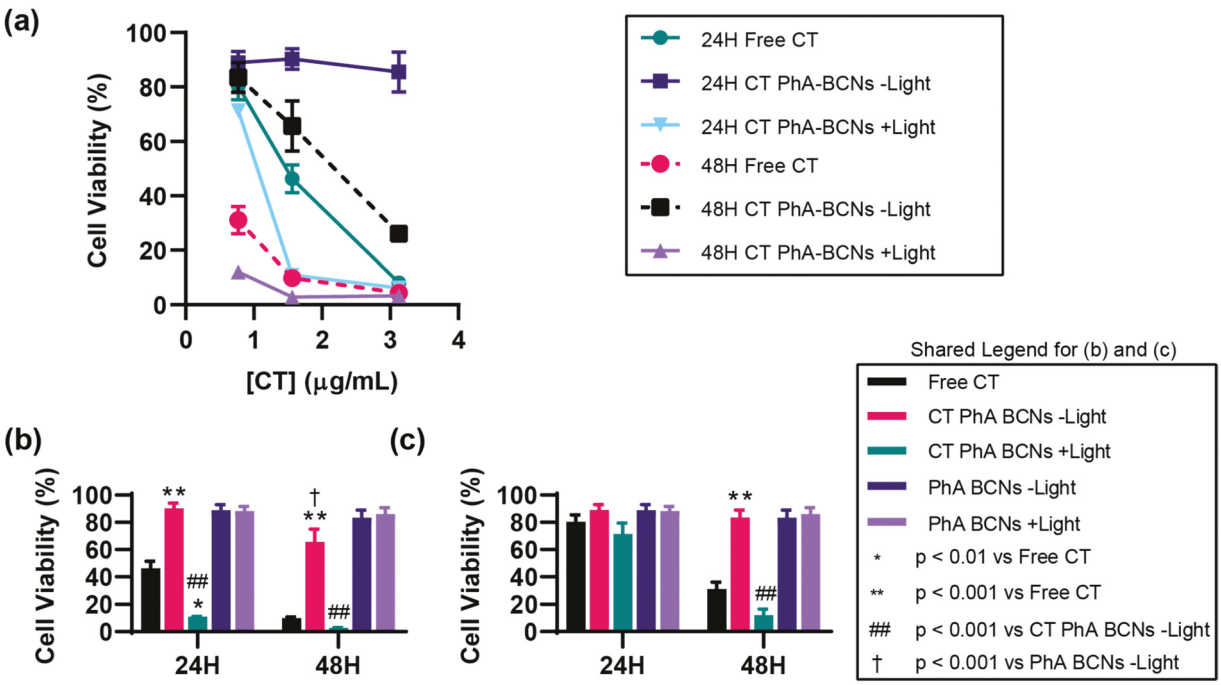

Fig. 4 Cytosolic delivery of cytotoxic cargo. (a) MTT viability assay of RAW 264.7 cells. Cells were treated with free camptothecin (CT) or PhA-BCNs loaded with CT at three concentrations (0.63, 1.56, and 3.1 μg mL^{-1}) for 8 h before a group was irradiated. Cells were irradiated for 2.5 minutes and incubated further to allow for the induction of cell death, either 24 or 48 h total. Statistical evaluation of the treatment groups at the (b) 1.56 μg mL^{-1} and (c) 0.63 μg mL^{-1} concentrations. PhA BCN −Light and +Light data at 24 and 48 h are duplicated between (b) and (c), displayed as such for ease of comparison. For all subfigures n = 4, error bars are s.d., statistical analysis by 2-way ANOVA.

FITC-BSA BCNs imaged in Fig. 1. In contrast, irradiated cells featured cytosolic release of the FITC-BSA, visible as a diffuse fluorescence throughout the cytosol.

Having demonstrated that PhA-BCNs are both minimally toxic and capable of triggered cytosolic delivery, we sought to assess their ability to protect cells from toxic cargo until on-demand release was triggered for off–on cytotoxicity. Camptothecin is an anti-cancer drug that functions by inhibiting DNA topoisomerase I, a protein present in the nucleus of cells.[24] Thus, camptothecin activity is dependent upon cytoplasmic and ultimately nuclear localization, which results in apoptosis and a rapid decrease in cell viability. Reasoning that the release of hydrophilic camptothecin from BCNs would occur upon oxidation of PEG-*b*-PPS, we loaded BCNs with camptothecin, with or without co-loading of PhA. Camptothecin-loaded PhA-BCNs (CT-PhA-BCNs) containing three concentrations of loaded drug were evaluated for cytotoxicity at 24 and 48 h after an 8 h incubation. Samples were either irradiated or non-irradiated and were also compared to free camptothecin. Non-irradiated CT-PhA-BCNs demonstrated no change in cytotoxicity at 24 h across the three camptothecin concentrations (Fig. 4a). This was statistically very similar to the non-toxic effects of PhA-BCNs as seen in Fig. 2f ($p = 0.091$). Non-irradiated CT-PhA-BCNs did show cytotoxicity at 48 h in a dose dependent manner, suggesting that by that timepoint there is enough release of drug to have a cytotoxic effect at the higher concentrations (Fig. 4a, dagger marker). In contrast to the non-irradiated encapsulated drug, free camptothecin demonstrated dose-dependent cytotoxicity at 24 h and high cytotoxicity regardless of concentration at 48 h. The irradiation of CT-PhA-BCNs, which resulted in cytosolic release of camptothecin, significantly reduced the viability of RAW 264.7 cells. At a camptothecin concentration of 1.56 μg mL^{-1}, irradiated CT-PhA-BCNs were significantly more cytotoxic than non-irradiated samples and at 24 h were even significantly more cytotoxic than free drug (Fig. 4b). At the lower 0.63 μg mL^{-1} concentration, significant cytotoxic effects were not seen for any treatment at 24 h (Fig. 4c). At 48 h however, both irradiated CT-PhA-BCNs and free CT were significantly more cytotoxic than non-irradiated CT-PhA-BCNs. These results demonstrate that at relevant drug concentrations, BCNs can safely retain drug within endosomal compartments until release is triggered, enhancing both the efficacy and selectivity of on-demand cytotoxicity.

Conclusions

In this work, we have demonstrated the first application of photo-sensitive polymeric BCNs by combining the photo-oxidative effects of PhA with oxidation-sensitive PEG-*b*-PPS. Light-induced oxidation of PEG-*b*-PPS BCNs resulted in a triggerable *in situ* morphological transition from bicontinuous to micellar nanostructures. The PEG-*b*-PPS polymer functioned as an ROS 'sponge' to inhibit the typical cytotoxicity and pro-apoptotic effects of PhA. Photo-oxidation of PhA-BCNs within the endosomes of cells resulted in the release of cargo into the cytosol. Such endosomal escape is a critical step in the delivery of many different types of cargo but is difficult to control in an off–on fashion with most triggerable polymeric nanocarriers, as rapid degradation can occur regardless of external stimulation.

Photosensitive self-assembled nanostructures are frequently employed to enhance localized delivery of systemically administered therapeutics. While photo-oxidation will significantly enhance delivery within irradiated tissues, self-assembled nanocarriers will still release payloads within off-target cells due to the degradative environments of the endolysosomal pathway. Here, we find that a bicontinuous nanoarchitecture enhances nanocarrier stability within cells, allowing PEG-*b*-PPS BCNs to resist degradation and stably retain payloads within cells under conditions that would otherwise rapidly cause disassembly for other self-assembled nanostructures of the same chemical composition, such as PEG-*b*-PPS polymersomes and filomicelles. We found that BCN protected cells from cytotoxic payloads, including pro-apoptotic photo-oxidizer pheophorbide A while under irradiation as well as the chemotherapeutic camptothecin. Interestingly, photo-oxidation induced a morphological transition of BCNs to a less stable micellar morphology, a process that we characterize *via* small-angle X-ray scattering and electron microscopy. This morphological transition induced cytosolic delivery of encapsulated camptothecin to both recover and enhance its cytotoxicity. To the best of our knowledge, this is the first demonstration of an inducible bicontinuous-to-micellar transition.

As BCNs inhibited cytoplasmic payload release under normal conditions without irradiation, this highlights the potential use of off–on triggerable photo-oxidation-sensitive platforms for improved control over cytosolic delivery. We demonstrated an advantage of this platform for the intracellular delivery of cytotoxic chemotherapeutics, significantly decreasing apoptosis under ambient conditions while maintain high efficacy upon light stimulation. Such platforms may serve to decrease off-target effects during nanotherapy as well as enhance cell-mediated drug delivery that requires payloads to remain within cells with minimal cytotoxicity, wherein cells can be loaded with therapeutics *ex vivo* and deliver payloads to specific organs and locations of disease.

Conflicts of interest

There are no conflicts to declare.

Acknowledgements

We acknowledge staff and instrumentation support from the Structural Biology Facility at Northwestern University, the Robert H Lurie Comprehensive Cancer Center of Northwestern University and NCI CCSG P30 CA060553. The Gatan K2 direct electron detector was purchased with funds provided by

the Chicago Biomedical Consortium with support from the Searle Funds at The Chicago Community Trust. SAXS experiments were performed at the DuPont-Northwestern-Dow Collaborative Access Team (DND-CAT) located at Sector 5 of the Advanced Photon Source (APS). DND-CAT is supported by Northwestern University, E.I. DuPont de Nemours & Co., and The Dow Chemical Company. This research used resources of the Advanced Photon Source, a U.S. Department of Energy (DOE) Office of Science User Facility operated for the DOE Office of Science by Argonne National Laboratory under Contract No. DE-AC02-06CH11357. This work made use of the EPIC facility of Northwestern University's NUANCE Center, which has received support from the Soft and Hybrid Nanotechnology Experimental (SHyNE) Resource (NSF ECCS-1542205); the MRSEC program (NSF DMR-1121262) at the Materials Research Center; the International Institute for Nanotechnology (IIN); the Keck Foundation; and the State of Illinois, through the IIN. This work made use of the IMSERC at Northwestern University, which has received support from the NSF (CHE-1048773); Soft and Hybrid Nanotechnology Experimental (SHyNE) Resource (NSF NNCI-1542205); the State of Illinois and International Institute for Nanotechnology (IIN). This work was supported by the Northwestern University – Flow Cytometry Core Facility supported by Cancer Center Support Grant (NCI CA060553). Imaging work was performed at the Northwestern University Center for Advanced Molecular Imaging generously supported by NCI CCSG P30 CA060553 awarded to the Robert H Lurie Comprehensive Cancer Center. This research was supported by the National Science Foundation (CBET-1806007 and CAREER Award no. 1453576), the National Institutes of Health Director's New Innovator Award (NHLBI 1DP2HL132390-01), and the National Institute of Allergy and Infectious Disease (NIAID 1R21AI137932-01A1).

Notes and references

1 J. S. Petschauer, A. J. Madden, W. P. Kirschbrown, G. Song and W. C. Zamboni, The effects of nanoparticle drug loading on the pharmacokinetics of anticancer agents, *Nanomedicine*, 2015, **10**, 447–463, DOI: 10.2217/nnm.14.179.

2 A. Z. Wang, R. Langer and O. C. Farokhzad, Nanoparticle delivery of cancer drugs, *Annu. Rev. Med.*, 2012, **63**, 185–198, DOI: 10.1146/annurev-med-040210-162544.

3 W. C. Zamboni, *et al.*, Best practices in cancer nanotechnology: perspective from NCI nanotechnology alliance, *Clin. Cancer Res.*, 2012, **18**, 3229–3241, DOI: 10.1158/1078-0432.CCR-11-2938.

4 S. Mura, J. Nicolas and P. Couvreur, Stimuli-responsive nanocarriers for drug delivery, *Nat. Mater.*, 2013, **12**, 991–1003, DOI: 10.1038/nmat3776.

5 E. Scarpa, *et al.*, Quantification of intracellular payload release from polymersome nanoparticles, *Sci. Rep.*, 2016, **6**, 29460, DOI: 10.1038/srep29460.

6 S. D. Allen, S. Bobbala, N. B. Karabin and E. A. Scott, On the advancement of polymeric bicontinuous nanospheres toward biomedical applications, *Nanoscale Horiz.*, 2019, **4**, 258–272, DOI: 10.1039/c8nh00300a.

7 S. D. Allen, S. Bobbala, N. B. Karabin, M. Modak and E. A. Scott, Benchmarking Bicontinuous Nanospheres against Polymersomes for in Vivo Biodistribution and Dual Intracellular Delivery of Lipophilic and Water-Soluble Payloads, *ACS Appl. Mater. Interfaces*, 2018, **10**, 33857–33866, DOI: 10.1021/acsami.8b09906.

8 S. Bobbala, S. D. Allen and E. A. Scott, Flash nanoprecipitation permits versatile assembly and loading of polymeric bicontinuous cubic nanospheres, *Nanoscale*, 2018, **10**, 5078–5088, DOI: 10.1039/c7nr06779h.

9 E. A. Scott, *et al.*, Dendritic cell activation and T cell priming with adjuvant- and antigen-loaded oxidation-sensitive polymersomes, *Biomaterials*, 2012, **33**, 6211–6219, DOI: 10.1016/j.biomaterials.2012.04.060.

10 S. Yi, *et al.*, Tailoring Nanostructure Morphology for Enhanced Targeting of Dendritic Cells in Atherosclerosis, *ACS Nano*, 2016, **10**, 11290–11303, DOI: 10.1021/acsnano.6b06451.

11 S. Allen, O. Osorio, Y. G. Liu and E. Scott, Facile assembly and loading of theranostic polymersomes via multi-impingement flash nanoprecipitation, *J. Controlled Release*, 2017, **262**, 91–103, DOI: 10.1016/j.jconrel.2017.07.026.

12 N. B. Karabin, *et al.*, Sustained micellar delivery via inducible transitions in nanostructure morphology, *Nat. Commun.*, 2018, **9**, 624, DOI: 10.1038/s41467-018-03001-9.

13 S. D. Allen, *et al.*, Celastrol-loaded PEG-b-PPS nanocarriers as an anti-inflammatory treatment for atherosclerosis, *Biomater. Sci.*, 2019, **7**, 657–668, DOI: 10.1039/c8bm01224e.

14 A. E. Vasdekis, E. A. Scott, C. P. O'Neil, D. Psaltis and J. A. Hubbell, Precision intracellular delivery based on optofluidic polymersome rupture, *ACS Nano*, 2012, **6**, 7850–7857, DOI: 10.1021/nn302122h.

15 O. Rajkovic, *et al.*, Reactive Oxygen Species-Responsive Nanoparticles for the Treatment of Ischemic Stroke, *Adv. Ther.*, 2019, **2**, 1900038, DOI: 10.1002/adtp.201900038.

16 S. Allen, M. Vincent and E. Scott, Rapid, Scalable Assembly and Loading of Bioactive Proteins and Immunostimulants into Diverse Synthetic Nanocarriers Via Flash Nanoprecipitation, *J. Vis. Exp.*, 2018, **138**, e57793.

17 W. H. Humphries and C. K. t. Payne, Imaging lysosomal enzyme activity in live cells using self-quenched substrates, *Anal. Biochem.*, 2012, **424**, 178–183, DOI: 10.1016/j.ab.2012.02.033.

18 P. Midoux, A. C. Roche and M. Monsigny, Quantitation of the binding, uptake, and degradation of fluoresceinylated neoglycoproteins by flow cytometry, *Cytometry*, 1987, **8**, 327–334, DOI: 10.1002/cyto.990080314.

19 T. M. Busch, K. A. Cengel and J. C. Finlay, Pheophorbide a as a photosensitizer in photodynamic therapy In vivo considerations, *Cancer Biol. Ther.*, 2009, **8**, 540–542, DOI: 10.4161/cbt.8.6.8067.

20 P. M. Tang, X. Z. Liu, D. M. Zhang, W. P. Fong and K. P. Fung, Pheophorbide a based photodynamic therapy induces apoptosis via mitochondrial-mediated pathway in human uterine carcinosarcoma, *Cancer Biol. Ther.*, 2009, **8**, 533–539, DOI: 10.4161/cbt.8.6.7694.

21 S. J. Yi, *et al.*, Surface Engineered Polymersomes for Enhanced Modulation of Dendritic Cells During Cardiovascular Immunotherapy, *Adv. Funct. Mater.*, 2019, 1904399, DOI: 10.1002/adfm.201904399.

22 H. K. Shete, R. H. Prabhu and V. B. Patravale, Endosomal escape: a bottleneck in intracellular delivery, *J. Nanosci. Nanotechnol.*, 2014, **14**, 460–474, DOI: 10.1166/jnn.2014.9082.

23 A. K. Varkouhi, M. Scholte, G. Storm and H. J. Haisma, Endosomal escape pathways for delivery of biologicals, *J. Controlled Release*, 2011, **151**, 220–228, DOI: 10.1016/j.jconrel.2010.11.004.

24 L. F. Liu, *et al.*, Mechanism of action of camptothecin, *Ann. N. Y. Acad. Sci.*, 2000, **922**, 1–10.